AGU PUBLICATIONS

Water Resources Research

TECHNICAL REPORTS: DATA

10.1002/2015WR018249

Sediment deposition within and around a finite patch of model vegetation over a range of channel velocity

Chao Liu[1,2] and Heidi Nepf[2]

[1]State Key Laboratory of Hydraulics and Mountain River Engineering, Sichuan University, Chengdu, China, [2]Department of Civil and Environmental Engineering, Massachusetts Institute of Technology, Cambridge, Massachusetts, USA

Key Points:
- The threshold for stem-turbulence production inside a vegetation patch is determined
- The effect of patch shape on flow and deposition patterns is investigated
- Criteria for enhanced deposition within vegetation patch are determined

Correspondence to:
C. Liu,
liuchaoscu@vip.qq.com

Citation:
Liu, C., and H. Nepf (2016), Sediment deposition within and around a finite patch of model vegetation over a range of channel velocity, *Water Resour. Res.*, *52*, 600–612, doi:10.1002/2015WR018249.

Received 15 OCT 2015
Accepted 2 JAN 2016
Accepted article online 7 JAN 2016
Published online 21 JAN 2016

Abstract The interaction between flow and vegetation creates feedbacks to deposition that vary with channel velocity. This experimental study describes how channel velocity and stem-generated turbulence influence the deposition within and around an emergent patch of model vegetation, with a particular focus on deposition within the patch. The Reynolds number threshold for stem-scale turbulence generation was determined using velocity spectra and flow visualization. At high channel velocity resuspension occurred in the bare regions of the channel and a nonuniform spatial distribution of net deposition was observed around and within the patch. In contrast, at low channel velocity there was no (or limited) resuspension and a uniform distribution of net deposition was observed around and within the patch. The deposition inside the patch was enhanced, relative to a bare-channel control, only when the following two criteria were met: (1) the absence of stem turbulence, and (2) the presence of sediment resuspension in the bare channel. Comparison to previous lab and field studies further support these criteria.

1. Introduction

Vegetation acts as an ecosystem engineer by modifying the flow, trapping and stabilizing sediment, and influencing morphological evolution [e.g., *Bennett et al.*, 2002; *Wu et al.*, 2005; *Gurnell et al.*, 2012; *Gurnell*, 2014]. Both *Cotton et al.* [2006] and *Sand-Jensen* [1998] demonstrated that the presence of macrophytes alters the spatial distribution of sediment deposition. Specifically, suspended sediment deposits within and downstream of vegetated regions, where the mean and turbulent velocities are diminished, such as the fully-developed region within a long patch of vegetation [*Zong and Nepf*, 2010], the wake behind a finite patch [*Takemura and Tanaka*, 2007; *Chen et al.*, 2012], and the secondary deposition zone behind neighboring patches [*Meire et al.*, 2014]. The deposition of fine sediment, which is rich in organic material and nutrients, promotes the expansion of the vegetated region [*Gurnell*, 2014], creating a feedback between vegetation-flow-deposition and further growth.

The feedback between vegetation and sediment retention varies temporally due to the remobilization of sediment during die back [*Heppell et al.*, 2009; *Sukhodolov and Sukhodolova*, 2009]. In addition, variability in channel velocity produces variations in suspended sediment concentration [*Wood and Armitage*, 1997]. During floods, the nonvegetated regions of a channel and regions of sparse vegetation suffer erosion, but sedimentation occurs in the regions with dense vegetation [*Asaeda et al.*, 2011]. The seasonal variation in river discharge and sediment availability produces a complex, shifting mosaic of landforms, which is dependent upon both the sediment characteristics and the magnitude and duration of the floods [*Cotton et al.*, 2006; *Gurnell and Petts*, 2002; *Naiman et al.*, 1993]. Taken together, these field observations indicate that both the channel velocity and the presence of vegetation can impact the spatial distribution of sedimentation.

In recent years, the impact of vegetation on flow and sediment erosion and deposition has been extensively investigated. In the field, vegetation often occurs in patches of finite length and width, and the pattern of flow around these patches has been linked to the pattern of deposition and erosion. For example, the lateral flow diversion around patches of finite width produces enhanced velocities laterally adjacent to the patch, where erosion is observed [*Bouma et al.*, 2007; *Vandenbruwaene et al.*, 2011; *Balke et al.*, 2012]. This negative feedback has been proposed as a constraint that keeps patches from expanding laterally [*van Wesenbeeck et al.*, 2008]. Other studies have linked wake flow structure with patterns of net deposition within the wake downstream of a patch. Directly downstream from the patch there is a near wake region in which both

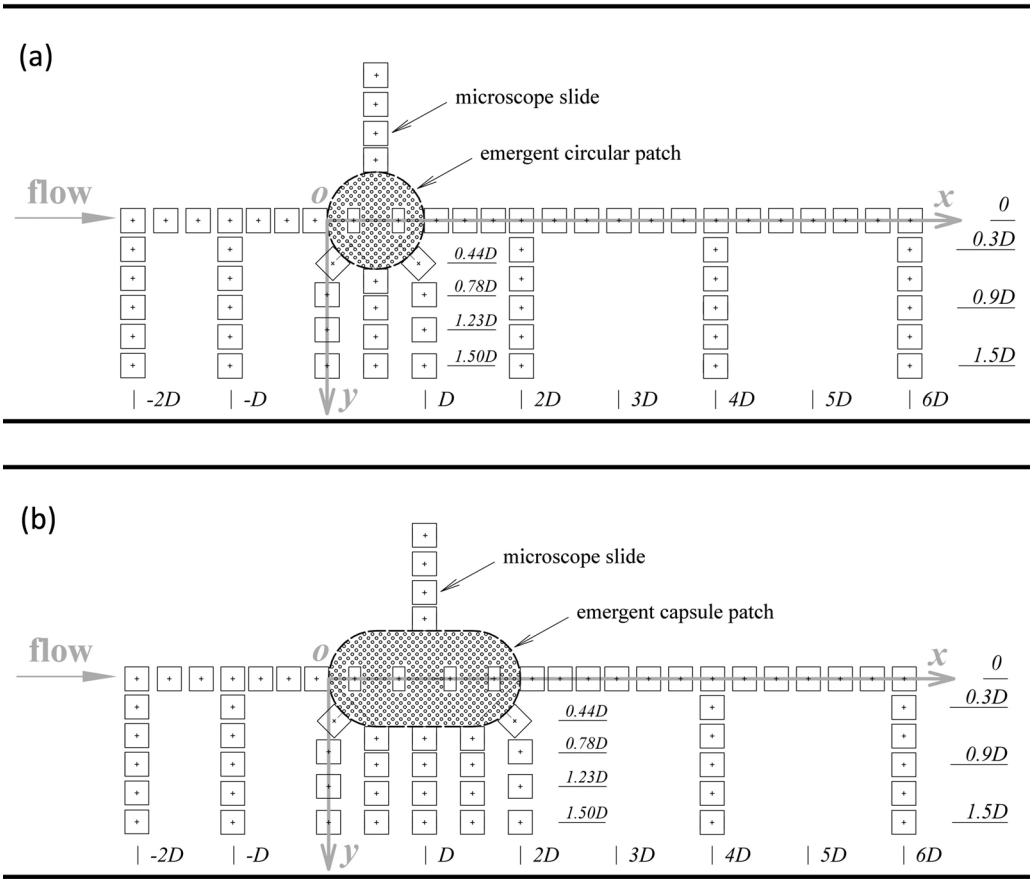

Figure 1. Top view of slide arrangement for (a) the circle patch (64 square slides and 2 rectangular slides); and (b) the capsule patch (64 square slides and 4 rectangular slides). The square slides are 2.5 cm × 2.5 cm, and the rectangular slides are 1.25 cm × 2.5 cm.

velocity and TKE are diminished, promoting deposition of fine material [*Takemura and Tanaka*, 2007; *Chen et al*., 2012]. Patch-scale turbulence, i.e., the von Karman vortex street, forms at a distance L_w downstream from the patch [e.g., see *Chen et al*., 2012, Figure 1]. Diminished net deposition, relative to a bare channel, has been observed in the region of the wake where the von-Karman vortex street is present [*Chen et al*., 2012; *Ortiz et al*., 2013]. Finally, within patches of vegetation both enhanced and diminished net deposition have been observed [e.g., *Bouma et al*., 2007; *Cotton et al*., 2006; *Follett and Nepf*, 2012; *Balke et al*., 2012]. While the retention of sediment within vegetation plays an important role in nutrient cycling within rivers [*Clarke*, 2002; *Jones et al*., 2012], and the evolution of coastal marshes [*Bouma et al*., 2007; *Balke et al*., 2012], it remains unclear what physical conditions are needed to promote deposition within a finite patch.

The presence of vegetation reduces the mean velocity, but may increase the turbulence level through the production of turbulence in the wakes of individual stems and branches [*Nepf*, 1999]. The presence of stem turbulence depends on the stem Reynolds number Re_d ($= ud/\nu$), where u is the velocity within the vegetation, d is the stem diameter, and ν ($= 0.01\ cm^2\ s^{-1}$) is the kinematic viscosity. Stem-scale turbulence has been observed at $Re_d > 200$ within natural river vegetation [*Naden et al*., 2006] and in many model canopies [*Liu et al*., 2008; *Ricardo et al*., 2014; *Zong and Nepf*, 2010, 2012] through analysis of velocity spectra and TKE profiles. In contrast, stem-generated turbulence is absent at low Re_d [*Tanino and Nepf*, 2008a].

Stem turbulence has been related to diminished deposition and erosion within model patches of vegetation. For example, *Follett and Nepf* [2012] found a positive correlation between the magnitude of stem-generated turbulence and the net erosion of sand within a patch of model emergent vegetation. Similarly, diminished net deposition has been observed within model laboratory patches [*Chen et al*., 2012; *Ortiz et al*., 2013], and net erosion of sand and mud substrates has been noted in patches of vegetation on intertidal flats [*Bouma et al*., 2007]. These previous studies suggest that stem-turbulence plays an important role

Table 1. Experimental Parameters and Conditions[a]

Case	U_0 (cm s^{-1})	C_D	C_DaD	Re_d	$Re_{d(x=0)}$	u_* (u_{*max}) (cm s^{-1})	Dep_{mean} (mg cm^{-2})	SD (mg cm^{-2})	Patch Configuration
1	9.1	3.1	16.0	154	220	0.64 (0.80)	1.31	0.67	Circle
2	7.1	3.4	17.5	121	170	0.50 (0.63)	1.60	0.62	Circle
3	6.2	3.6	18.4	107	150	0.44 (0.55)	1.85	0.59	Circle
4	5.1	4.0	20.4	86	120	0.36 (0.45)	2.19	0.40	Circle
5	3.1	5.5	28.1	49	75	0.22 (0.27)	2.23	0.11	Circle
6	1.0	11.9	61.4	17	24	0.07 (0.09)	2.24	0.06	Circle
7	0	0	0	0	0	0	1.40	0.10	Circle
8	9.1	3.5	17.8	116	220	0.64 (0.86)	0.97	0.54	Capsule
9	9.1					0.64	1.45	0.18	None
10	6.2					0.44	2.34	0.08	None
11	3.1					0.22	2.24	0.07	None
12	0					0	1.40	0.13	None
13	9.1	draining only				0.64	0.12	0.02	None

[a]U_0 is the channel velocity. Re_d is the mean stem Reynolds number inside the patch. $Re_{d(x=0)}$ is the stem Reynolds number at the leading edge of the patch ($x = 0$). Case 9 to 12 were control experiments (no patch). Case 13 evaluated the net deposition during 20-min draining. Channel shear velocity $u_* = \sqrt{c_f}U_0$, in which $c_f = 0.005$ [*White and Nepf*, 2007]. Maximum shear velocity $u_{*max} = 1.25\sqrt{c_f}U_0$ for Cases 1–7, and $= 1.33\sqrt{c_f}U_0$ for Case 8. Dep_{mean} was the mean of the net deposition over entire channel, and SD was the spatial standard deviation.

in deposition within a vegetation patch. Because of the role of in-canopy deposition in nutrient cycling [e.g., *Chambers et al*., 1989] and landscape evolution [e.g., *Bouma et al*., 2007] it is important to understand what flow conditions promote in-canopy deposition. The focus of the present study is to define the conditions for which enhanced deposition may occur within a finite patch of vegetation, and to provide guidance for making that evaluation in the field.

2. Experiment Methods

Experiments were conducted in a 3.75 m long, 0.4 m wide recirculating Plexiglas flume with a 2.84 m long test section. The bed of the flume was horizontal. A pump with variable speed motor provided a maximal discharge of 3.8 L per second. The flow depth was $H = 14.0 \pm 0.1$ cm, and the channel velocity (U_0) was varied between 0 and 9.1 cm s^{-1}. To explore the influence of patch length, two patch geometries were considered: circular, with patch diameter $D = 10$ cm, and elongated, with width D and length $2D$. The design of the elongated (or capsule) patch is discussed in the last paragraph of this *Experimental Methods* section. The model patch of emergent vegetation was constructed at the center of the channel using smooth wooden, circular dowels with diameter $d = 0.36$ cm. The cylinders were fitted into a PVC baseboard with a staggered array of holes. The stem density was $n = 1.43$ cm^{-2}. The frontal area per volume, a ($= nd$), was 0.51 cm^{-1}, and the solid volume fraction, φ ($= \pi ad/4$), was 0.15. For both geometries the patch width was 10 cm, so that the patch blocked 25% of the channel width. The drag coefficient within the patch, C_D, was estimated from *Tanino and Nepf* [2008b, equation (5)]. Based on φ and maximum Re_d, $C_D = 3.1$, yielding $C_DaD = 16$, which corresponded to high flow blockage ($C_DaD > 4$) [*Chen et al*., 2012]. Experimental parameters for all cases are shown in Table 1.

Instantaneous measurements of longitudinal velocity, $u(t)$, lateral velocity, $v(t)$, and vertical velocity, $w(t)$, were measured by a Nortek Vectrino, and the raw data were despiked following the method of *Goring and Nikora* [2002]. The threshold velocity above which stem-generated turbulence occurred (i.e., corresponding to Re_{dc}) was determined by analyzing the velocity spectra (S_{vv}) measured at the point closest to the downstream edge of the patch ($x = 11.3$ cm). S_{vv} was obtained by processing instantaneous velocities using Welch's method, as described in the Matlab toolbox. The production of stem-scale turbulence was identified by a peak in the spectra corresponding to the frequency of vortex shedding from a circular cylinder, which is described by the Strouhal number, $St = fd/U_e$, in which f is the vortex-shedding frequency, and U_e is the velocity measured at the point used for the spectral analysis (see details given in *Zong and Nepf* [2012]). For an isolated cylinder $St = 0.12$ to 0.21, increasing with Re_d over the range $Re_d = 50$ to 1000 [*Norberg*, 1994]. Similarly, *Zong and Nepf* [2012] measured $St = 0.14$ to 0.24 directly behind model patches of vegetation with different patch diameter and cylinder density and within which $Re_d = 250$ to 470. Based on these

studies, we expect stem-generated turbulence will manifest as a peak in the S_{vv} spectra at frequency $f = StU_e/d$, with $St = 0.1$ to 0.2.

The presence of stem-generated turbulence within the model patch was also evaluated by imaging the evolution of a fine line of tracer (fluorescein) within the patch. A UV light was positioned above the flume to excite the fluorescein, which was injected continuously from a horizontal needle located 1 cm upstream of the patch ($x = -1$ cm) and 4 cm below the water surface ($z = 10$ cm) at a constant rate chosen so that the tracer velocity at the needle tip was close to or less than the ambient velocity, to avoid producing additional turbulence during the injection. A Canon 5D Mark III camera fixed above the center of the circular patch ($x = 5$ cm and $y = 0$ cm) captured the tracer motion. To avoid light reflection from the water surface, the images were taken in a totally dark environment.

The deposition experiments were conducted using a model sediment of glass spheres ($d_{10} = 1.5$ μm, $d_{50} = 5.6$ μm and $d_{90} = 13.3$ μm) from Potters Industry (Valley Forge, PA) with a density of $\rho_p = 2.5$ g cm^{-3}. The particle settling velocity ($w_s = 0.002$ cm s^{-1}) was estimated using the following equations from *Cheng* [1997], which covers particle diameters $d_p = 1 \times 10^{-4}$ to 1 cm,

$$\frac{w_s d_p}{\nu} = \left(\sqrt{25 + 1.2 d_*^2} - 5\right)^{1.5} \tag{1}$$

in which d_p is the particle diameter ($= d_{50}$) and d_* is the dimensionless particle parameter

$$d_* = \left[\frac{(\rho_p - \rho_w) g}{\rho_w \nu^2}\right]^{1/3} d_p \tag{2}$$

with ρ_w the water density, and g the gravitational acceleration. For the model particles $d_* = 0.13$. The model particles were scaled to match the ratio of settling velocity to channel shear velocity (u_*) observed for fine organic matter in streams, for which $w_s/u_* = 0.002$ to 0.3. For the model particles $w_s/u_* = 0.003$ to 0.029. The particle size was not scaled. A detailed discussion of particle scaling is provided in *Ortiz et al*. [2013].

In a bare channel, the critical bed shear stress (τ_c) describes the initiation of sediment motion, i.e., resuspension, with u_{*c} the critical shear velocity, and τ_{*c} the Shields parameter.

$$\tau_c = \rho_w u_{*c}^2 = \tau_{*c}(\rho_p - \rho_w) g d_p \tag{3}$$

For $d_* < 0.3$, $\tau_{*c} = \frac{1}{2}\tan 30^\circ = 0.29$ [*Julien*, 1995], so $u_{*c} = 0.49$ cm s^{-1} for the model particles. We defined two shear velocities to describe the bed stress present in the channel. First, the channel shear velocity (u_*) was estimated from the channel velocity (U_0), specifically $u_* = \sqrt{c_f} U_0$, with bed friction coefficient $c_f = 0.005$, based on previous experiments using the same baseboards [*White and Nepf*, 2007]. We note that the flow in the test section is not fully developed. A vertical profile of streamwise velocity taken 20 cm upstream of the patch (data not shown) indicated that the bottom boundary layer was roughly 2 cm. This does not limit the results, because fully developed flow is not always present around vegetation patches in the field. However, this does introduce some uncertainty in our estimate of u_*, because the bed-friction coefficient (c_f) was measured for fully developed flow over the same baseboards, for which the boundary layer would be larger. Therefore, the equation $u_* = \sqrt{c_f} U_0$ may under predict the true local value of u_*. In cases with model patches (Case 1 to 8), we also calculated the maximum shear velocity ($u_{*\max} = \sqrt{c_f} U_{\max}$), which occurred in the region adjacent to the patch, where the velocity increased to a local maximum $U_{max} = 1.25U_0$ and $1.33U_0$ for the circular and capsule patches, respectively (data not shown).

Table 2. Parameters of Model Patch in our Experiments and the Published Literature[a]

	a (cm^{-1})		φ					
Source	Sparse	Dense	Sparse	Dense	D (cm)	L (cm)	d (mm)	Patch Configeration
Our experiments		0.51		0.15	10		3.6	Circle
Chen et al. [2012]	0.06	0.20	0.03	0.11	42		6.4	Circle
Zong and Nepf [2010]	0.04	0.20	0.02	0.10	40[b]	800	6.0	Rectangle

[a] a is the frontal area per volume. φ is the solid volume fraction. D is the patch diameter. d is the stem diameter.
[b] For the rectangular patch, D was the width and L was the length.

To measure net deposition, we arranged 64 square glass slides (2.5 cm × 2.5 cm) around the patch, with 2 and 4 rectangular slides (1.25 cm × 2.5 cm) inside the circular and capsule patch, respectively (see Figure 1). A few stems were moved to accommodate the slides, and these were placed elsewhere in the patch, so that the overall stem density was not changed. Dry slides were initially weighed and then placed on the channel bed with no flow. The pump speed was slowly increased to the target discharge, after which 93.4 g of particles was mixed in a large plastic measuring cup. The slurry was gently poured into the downstream tank and transported to the upstream tank by the pump. The particles were mixed to a uniform concentration within 15 min. Once mixed, the concentration was 105 g m^{-3}. The experiment ran for 4 h, which was much longer than the initial mixing time. This was a closed, recirculating system, so that both the flow and particles were recirculating during experiment. After 4 h the pump was slowly stopped (over 30 s) to prevent wave generation, and the water was slowly drained, taking 20 min. After draining, the slides were allowed to dry for 12 h, with four heat lamps placed along the flume to accelerate drying, after which the slides were placed in an oven at 50°C for 4 h to remove moisture. Finally, the slides were reweighed and the net deposition at each position was calculated by the difference in weight before and after the experiment. Each condition was repeated at least two times to evaluate the uncertainty. In Case 7 (circular patch) there was no current ($U_0 = 0$ cm s^{-1}). In this case the pump was run with an initial channel velocity ($U_0 = 3.1$ cm s^{-1}) for 15 min to mix the particles, after which the pump was slowly stopped and the still water with suspended sediment was left for 4 h. Control experiments with no patch (Case 9, 10, 11, 12) were conducted with the same flow conditions as Case 1, 3, 5, 7, respectively (see Table 1). The deposition that occurred during the 20-min draining period was evaluated in Case 13 (no patch) by placing five additional slides in the flume just before draining.

The elongated capsule patch was designed to create in-patch conditions without stem-generated turbulence at the highest channel velocity ($U_0 = 9.1$ cm s^{-1}). The design method described here can also provide a framework for evaluating in-patch flow conditions in the field. Previous studies were used to describe the velocity evolution at the leading edge, from which we found the distance from the leading edge at which stem-generated turbulence should be eliminated (L_t). In the field, the patch length, L, must be greater than L_t to produce conditions with enhanced deposition within the patch. As described below, velocity spectra and flow visualization determined the critical Reynolds number below which stem-generated turbulence was absent ($Re_{dc} = 120$). We designed a patch for which Re_d dropped below $Re_{dc} = 120$. With model stem diameter $d = 0.36$ cm, the target velocity for L_t was $U_{L_t} = (\nu/d)Re_{dc} = 3.3$ cm s^{-1}.

Figure 2 describes the longitudinal velocity profiles within three patches: circular, elongated capsule and infinite. We consider high flow-blockage patches ($C_D aD > 4$), for which the velocity decays over the adjustment length-scale $X_D = 3.5D$ [*Rominger and Nepf*, 2011, equation (4.5)], at which point the flow reaches the fully-developed interior velocity (U_{X_D}), which can be estimated from *Rominger and Nepf* [2011, equation (4.10)],

$$\frac{U_{X_D}}{U_0} = \sqrt{2c_f \frac{(1-\phi)}{C_D aD}}, \tag{4}$$

For our patch $X_D = 35$ cm and $U_{X_D}/U_0 = 0.025$. To simplify the analysis, we approximated the observed exponential velocity decay at the leading edge of a patch [*Rominger and Nepf*, 2011] as a linear decay from $U_{x=0}$ to U_{X_D} over distance X_D (Figure 2). Importantly, *Chen et al.* [2013] showed that the velocity decay was independent of patch length, even for patches shorter than X_D, so this analysis is valid for $L_t < X_D$. Assuming linear velocity decay, L_t was calculated by solving

$$\frac{(U_{x=0} - U_{X_D})}{X_D} = \frac{(U_{x=0} - U_{L_t})}{L_t} \tag{5}$$

The velocity at the leading edge, $U_{x=0}$, was estimated using equation (4) in *Chen et al.* [2012]

$$\frac{U_{x=0}}{U_0} = 1 - \frac{1}{2}\alpha A C_D aD \tag{6}$$

in which α and A are parameters estimated by *Chen et al.* [2012], $\alpha A = 0.04$, so that $U_{x=0}/U_0 = 0.68$. From equations (5) and (6), $L_t = 17$ cm. The elongated patch was chosen to be longer than L_t, specifically 20 cm.

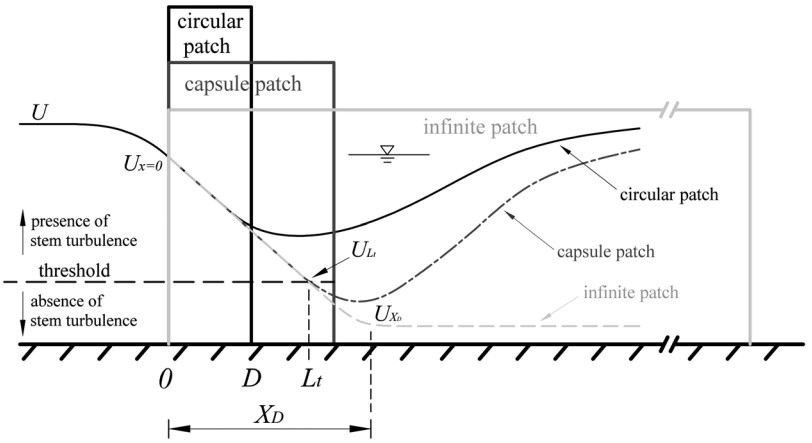

Figure 2. The distributions of normalized velocity, U/U_0, (vertical axis) as a function of streamwise distance (horizontal axis) for a circular patch (diameter D), a capsule patch (width D, length $2D$), and a patch of infinite length (width D). The leading edge of all patches is at x = 0. X_D is the interior adjustment length, which is the same for all three patches [*Chen et al.*, 2013]. L_t is the distance from the leading edge at which the velocity reaches the value for which $Re_d = Re_{dc}$, denoted by horizontal "threshold" dashed line. The velocities $U_{x=0}$, U_{L_t} and U_{X_D} are located at $x = 0$, L_t and X_D, respectively.

3. Results

3.1. Threshold for Stem-Generated Turbulence

Using the expected Strouhal number, $St = fd/U_e = 0.1$ to 0.2, we examined the velocity spectra for frequency peaks in the range $f = [0.1 \text{ to } 0.2]U_e/d$. The individual cases were classified with the Reynolds number at the leading edge, $Re_{d(x=0)}$ ($= U_{x=0}\, d/\nu$), which was the highest value of Re_d within the patch. A distinct peak was observed at $f = 0.8$, 0.7 and 0.3 Hz in Cases 1, 2 and 3, respectively, corresponding to $Re_{d(x=0)} = 220$, 170, 150, respectively. The peak was less obvious in Case 4 ($Re_{d(x=0)} = 120$), and was completely absent in Case 5 ($Re_{d(x=0)} = 75$), suggesting that the threshold for stem-generated turbulence was crossed near $Re_{d(x=0)} = 120$. A similar threshold was revealed in the tracer visualization (Figure 3). The motion of individual stem-scale vortices was visible for Case 1 ($Re_{d(x=0)} = 220$) and Case 2 ($Re_{d(x=0)} = 170$), and for these cases small-scale mixing quickly blended the tracer into a visually smooth field of color. For example, examine the region within the red dashed circle (region A) and in the wake of the patch in Figure 3a (Case 1, $Re_{d(x=0)} = 220$). The mixing of tracer was similar in Case 3 ($Re_{d(x=0)} = 150$) and Case 4 ($Re_{d(x=0)} = 120$), but both exhibited less mixing than Case 1 (Figure 3a). For example, in Case 4 (Figure 3b) while some blurring occurred, edges of individual filaments were still visible both within region A and in the wake. Finally, for $Re_{d(x=0)} = 75$ (Case 5, Figure 3c), distinct filaments of tracers were clearly observed in region A, consistent with the absence of stem-scale frequency peak in the spectra. Taken together, the velocity spectra and tracer visualization (Figure 3) suggested a gradual elimination of stem-generated turbulence for $Re_{d(x=0)} \leq 120$. Based on this, we defined $Re_{dc} = 120$.

3.2. Sediment Deposition

From the settling velocity ($w_s = 0.002$ cm s^{-1}) the settling time-scale was estimated to be $H/w_s \approx 7000$ s or 1.9 h ($H = 14.0 \pm 0.1$ cm). Therefore, in the absence of resuspension, we expected most of the particles to settle within the experiment time (4 h). This was tested in Case 12 with no current. The initial sediment concentration was 105 g m^{-3} throughout the flume. If all suspended particles in the test section settled to the bed, the deposition would be 1.47 mg cm^{-2} ($= 0.14$ m $\times$ 105 g m^{-3}). After 4 h, the observed net deposition was 1.40 mg cm^{-2}, indicating 95% particles had deposited on the channel, consistent with the expectation.

The additional deposition that occurred during the 20-min draining process was measured by adding five new slides just before draining (Case 13 in Table 1). The deposition during draining, 0.12 ± 0.02 (SD) mg cm^{-2} (Table 1), was just 5% to 12% of the deposition measured over the full experiment (4 h + 20 min draining). Importantly, the deposition measured during draining was fairly uniform ($SD/Dep_{mean} = 16\%$).

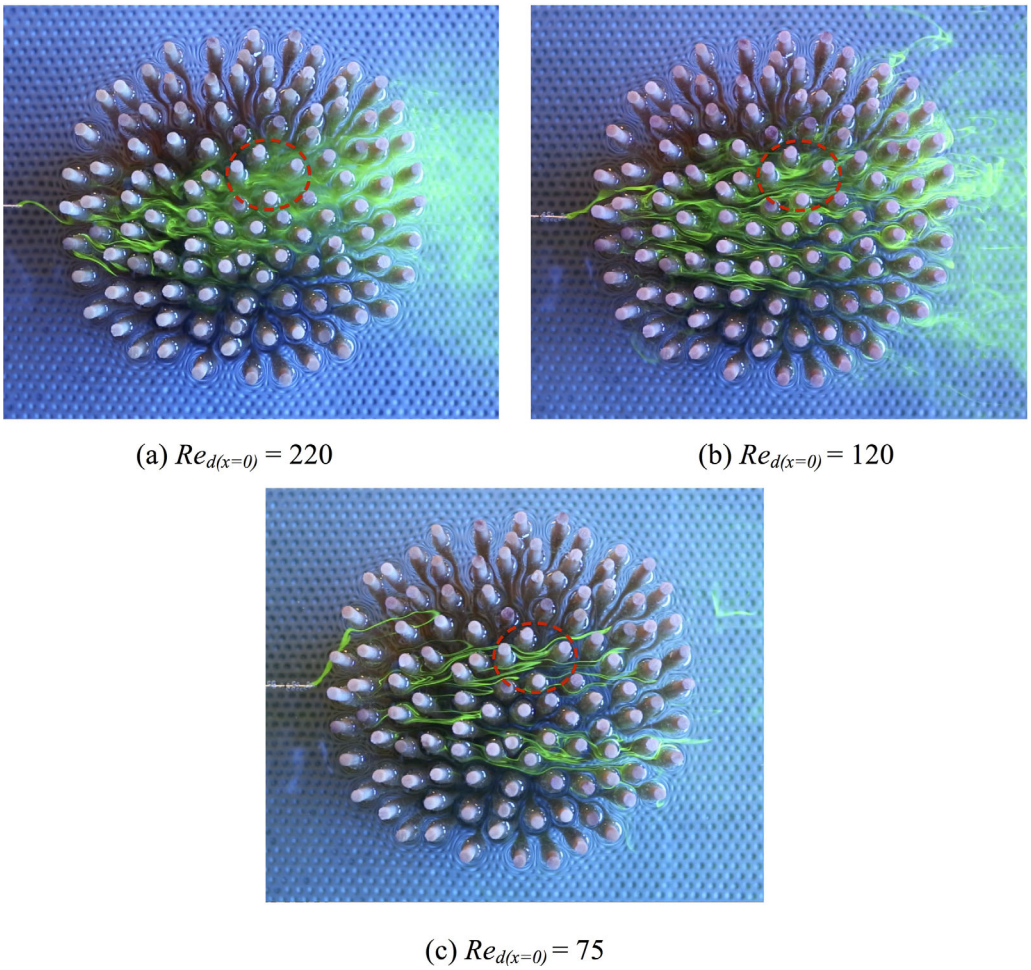

Figure 3. Flow visualization using UV light and fluorescein in (a) Case 1; (b) Case 4; and (c) Case 5. Flow direction from the left to right. Injection point directly upstream of patch. The needle tip is visible at left edge of images. Camera positioned above the centre of the patch. The diameter of this circular patch was $D = 10$ cm. Region A indicated by a red dashed circle.

Therefore, we were confident that spatial patterns in net deposition observed in the cases with flow were associated with the conditions imposed during the 4 h experiment and not during the draining process.

With the pump running, the settling time-scale (7000 s) was much larger than the transit time through the test-section ($L/U_0 \approx 30$ to 290 s, $L = 2.84$ m). In addition, the sediment was remixed each time it passed through the pump (every 200 to 500 s), so that the concentration within the test section (C) was assumed to be uniform, producing a spatially-uniform deposition rate w_sC. Therefore, spatial patterns in net deposition were attributed to differences in resuspension. First, consider the control cases without patches (Case 9 to 12, Table 1). When $u_* < u_{*c}$, resuspension should be absent. If only deposition occurred, the accumulation of mass at the bed should be independent of the channel velocity, because H and w_s were the same for all cases. Consistent with this, the net deposition in Case 10 (2.34 ± 0.08 mg cm^{-2}) and Case 11 (2.24 ± 0.07 mg cm^{-2}) were the same within uncertainty. These were the maximum net deposition for cases with current, which was higher than the net deposition with no current (Case 12, 1.40 ± 0.13 mg cm^{-2}). This can be explained by the fact that little deposition occurred in the pipes, so that as the water continuously circulated, all of the particles originally added to the flume were available to deposit in the test section. In contrast, for the zero channel velocity case, only the particles originally in the test section were available to deposit in the test section. Finally, in the highest channel velocity control case (Case 9, $U_0 = 9.1$ cm s^{-1}), $u_* > u_{*c}$ (Table 1), indicating that resuspension should be active. Consistent with this, the net deposition in Case 9 (1.45 ± 0.18 mg cm^{-2}) was diminished, due to the resuspension, relative to the control cases at lower channel velocity (Case 10 and 11).

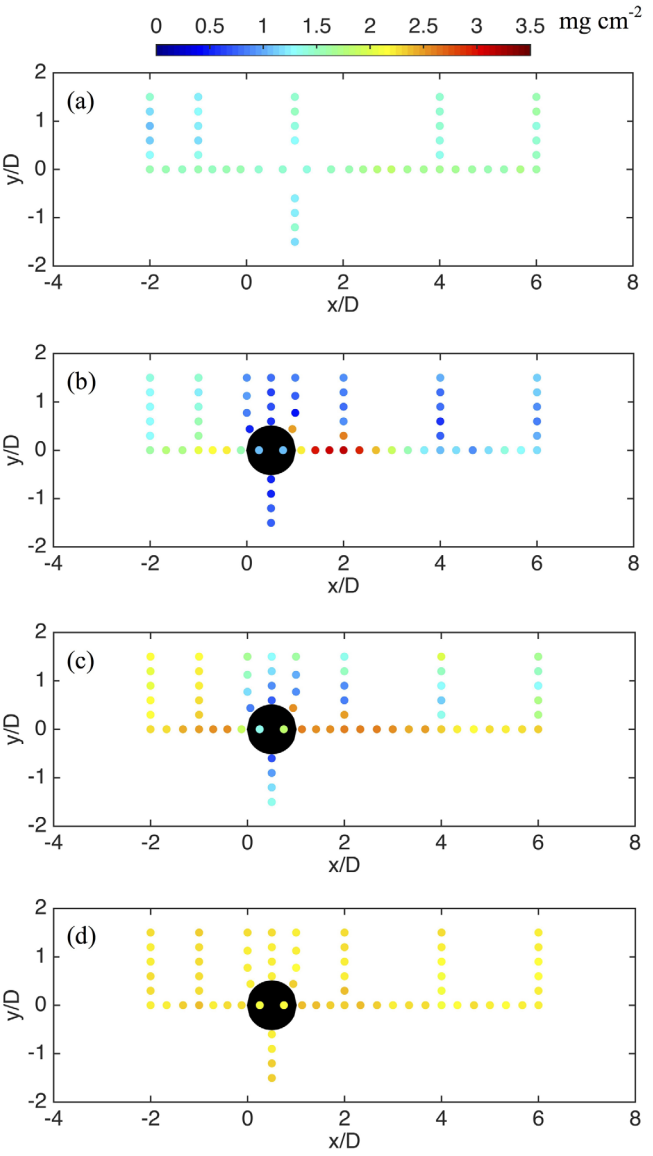

Figure 4. Spatial distribution of net deposition in (a) Case 9 (no-patch control, $U_0 = 9.1$ cm s^{-1}), (b) Case 1 ($U_0 = 9.1$ cm s^{-1}), (c) Case 3 ($U_0 = 6.2$ cm s^{-1}), and (d) Case 6 ($U_0 = 1.0$ cm s^{-1}). Points located at measurement positions. Color indicates magnitude of net deposition (mg cm^{-2}), according to color bar. When present the circular patch is denoted by a black solid circle.

The spatial distribution of net deposition for one no-patch control and three patch cases are shown in Figure 4. The black circle denotes the patch, and the color bar indicates the magnitude of net deposition in mg cm^{-2}. First, consistent with the flow symmetry, the net deposition was symmetric across the flume and patch centerline. Second, a distinct spatial pattern in net deposition was observed in the patch cases with high channel velocity (Case 1 and 3, Figures 4b and 4c). In the region adjacent to the patch, where the velocity was elevated to $1.25U_0$, the net deposition was diminished relative to the wake region downstream from the patch, where the flow was reduced to $0.1U_0$ to $0.3U_0$. For example, in Case 1, the net deposition over the majority of the channel was less than 1.8 mg cm^{-2}, but a local maximum in net deposition (3.12 mg cm^{-2}) occurred at $x/D = 2$ within the wake, consistent with low velocity and TKE at this location (data not shown). Importantly, the wake deposition was higher than that observed in the control at the same channel velocity (Case 9, Figure 4a, 1.45 mg cm^{-2}), indicating that the patch wake enhanced the deposition of the suspended particles. Similarly, in Case 3, net deposition was diminished adjacent to the patch (blue dots in Figure 4c), while the net deposition in the wake (orange dots) was elevated relative to the control (Case 10, see Dep_{mean} in Table 1). In contrast, for the lowest channel velocity case, $U_0 =$ 1.0 cm s^{-1} (Case 6, Figure 4d), the net deposition was spatially uniform. Finally, the net deposition inside the patch was either diminished relative to the open channel or had the same value as the open channel. Diminished net deposition within the patch (Case 1 and 3, Figures 4b and 4c) was attributed to stem-generated turbulence, which was confirmed by velocity spectra and flow visualization, as discussed in section 3.1. In Case 6 (Figure 4d) the velocity throughout the patch was low enough to be below the critical Reynolds number and the net deposition was equal to the deposition in the surrounding open channel. This was attributed to both the lack of stem-generated turbulence ($Re_{d(local)} < Re_{dc}$), and the lack of resuspension in the open channel, i.e., throughout the flume only deposition occurred.

To further investigate the spatial pattern of net deposition, we divided the domain into three regions (see Figure 5): (1) within the circular patch (triangles), (2) laterally adjacent to the patch (squares), and (3) maximal deposition in the wake (circles). In Figure 5 the critical shear velocity u_{*c} (= 0.49 cm s^{-1}) is denoted by a vertical dashed line, and a vertical grey bar marks the critical Reynolds number $Re_{dc} = 120$. First, for low channel velocity ($U_0 \leq 3.1$ cm s^{-1}), the net deposition in the three regions was the same within uncertainty,

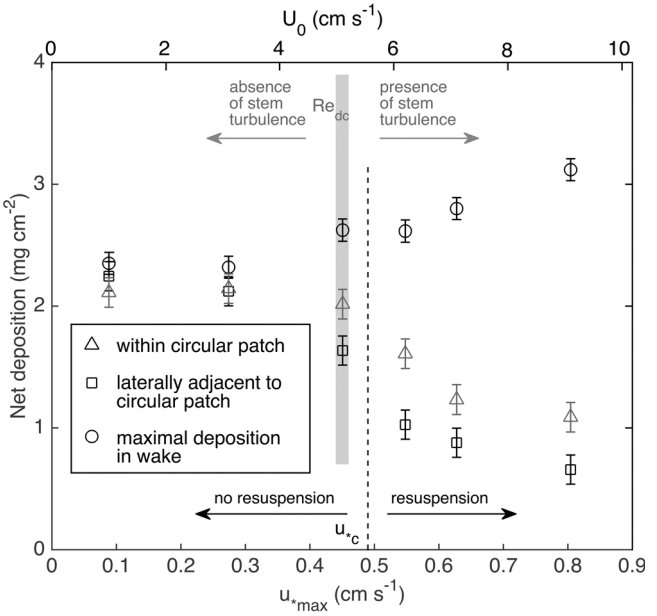

Figure 5. Net deposition as a function of maximum shear velocity ($u_{*max} = 1.25\sqrt{c_f}U_0$) in the open channel and upstream channel velocity (U_o) in three regions: (1) within the circular patch (△); (2) laterally adjacent to the circular patch (□), and (3) the maximal deposition in the wake (○). The vertical, dashed line indicates the critical shear velocity (u_{*c} = 0.49 cm s^{-1}). The vertical grey bar indicates the threshold stem Reynolds number (Re_{dc} = 120).

consistent with the lack of resuspension implied by $u_{*max} \leq u_{*c}$. Second, as u_{*max} surpassed u_{*c}, the net deposition adjacent to the patch progressively decreased, reflecting resuspension (squares, Figure 5). Importantly, as resuspension increased adjacent to the patch, net deposition within the wake (circles, Figure 5) increased ($U_0 \geq 5.1$ cm s^{-1}). That is, particles inhibited from depositing in the adjacent region became available to deposit in the wake. Third, within the patch (triangles), the net deposition was the same within uncertainty for $U_0 \leq 5.1$ cm s^{-1}, roughly corresponding to $Re_{d(x=0)} \leq Re_{dc}$. For $U_0 > 5.1$ cm s^{-1} (i.e., $Re_{d(x=0)} > Re_{dc}$) the patch net deposition (triangles) decreased, even as the net deposition in the wake (circles) increased. We attributed this to the onset of stem-generated turbulence within the patch, which inhibits deposition. Given the trends in Figure 5, we posit the following criteria for enhanced net deposition to occur within a patch: (1) the absence of stem turbulence ($Re_{d(local)} < Re_{dc}$), and (2) resuspension in the open channel ($u_* > u_{*c}$) to provide suspended load to the patch.

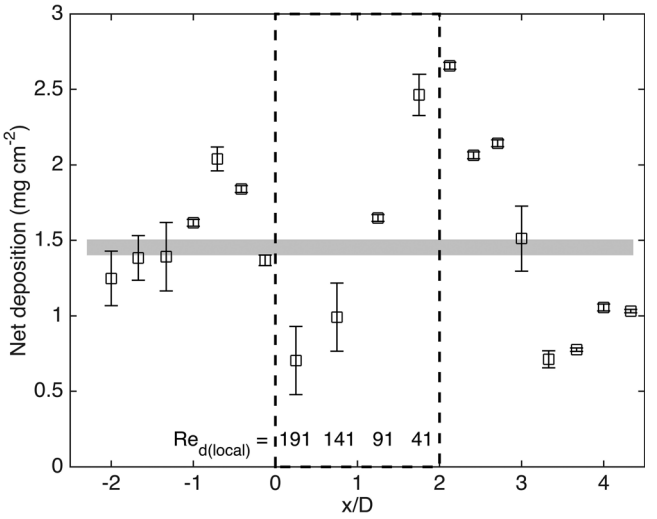

Figure 6. Longitudinal profile of net deposition along the centerline of capsule patch (Case 8). The vertical dashed lines indicate the leading ($x/D = 0$) and trailing ($x/D = 2$) edge of the patch. The grey horizontal bar denotes the net deposition in the control with no patch, and its width represents the spatial standard deviation in the control. The error bar for each point represents the difference between two replicate experiments. Values of $Re_{d(local)}$ inside the patch indicated for positions x/D = 0.25, 0.75, 1.25 and 1.75. Because the ADV could not be placed in the patch, the variation in velocity, and thus $Re_{d(local)}$, inside the patch was estimated using a linear interpolation of velocity between the leading and trailing edges of the patch.

To test the above criteria, we examined an elongated patch (Case 8, U_o = 9.1 cm s^{-1}) designed to produce $Re_d < Re_{dc}$ in the patch with resuspension in channel ($u_{*max} > u_{*c}$). The net deposition on the centerline of the elongated patch is presented in Figure 6. The net deposition in the patch was diminished relative to the control (marked in Figure 6) near the leading edge at positions for which $Re_{d(local)} > 120$ (values marked in figure), suggesting that stem-scale turbulence inhibited deposition in this region. Farther from the leading edge (x/D = 1.25 and 1.75), $Re_{d(local)} < Re_{dc}$ and net deposition was significantly enhanced above the control. These points support the dual criteria, that both $u_{*max} > u_{*c}$ and $Re_{d(local)} < Re_{dc}$ must be met to produce enhanced net deposition within a patch.

To further test these criteria, we combined observations from the present study with those from sparse and

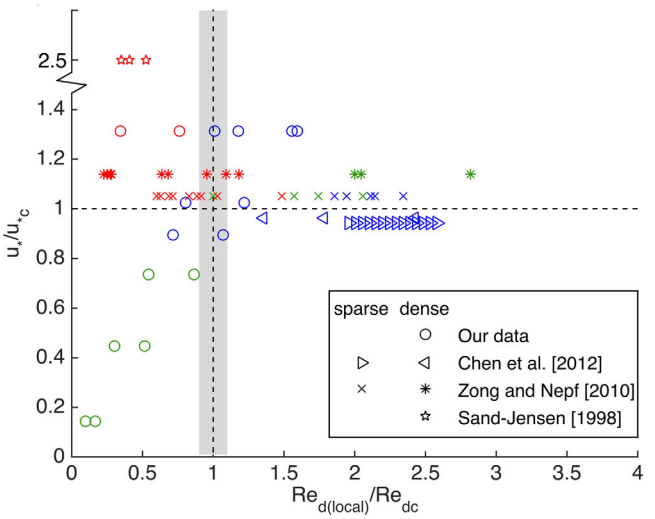

Figure 7. Parameter space defined by normalized channel shear velocity (u_*/u_{*c}) versus normalized patch Reynolds number ($Re_{d(local)}/Re_{dc}$). The symbol color indicates whether net deposition inside the patch was less than (blue), the same as (green), or more than (red) the open channel control. The grey vertical bar indicates $Re_{d(local)}/Re_{dc} = 1$, with uncertainty. Additional details in Table 2.

dense patches considered by *Zong and Nepf* [2010] and *Chen et al.* [2012]. The critical Reynolds numbers (Re_{dc}) for the patches in *Zong and Nepf* were inferred from the longitudinal (x) profiles of *TKE* provided in that paper [*Zong and Nepf*, 2010, Figure 4e]. The *TKE* was elevated above the open channel (TKE_0) at the leading edge of the patch and declined with distance from the leading edge. We identified the position (x) at which $TKE(x) = TKE_0$ inside the patch, for which we assumed stem-generated turbulence was no longer significant. The velocity at this x position [*Zong and Nepf*, 2010, Figures 4a and 4c] was used to define $Re_{dc} = 132 \pm 12$ in the dense patch ($\phi = 0.1$, comparable to the density in this paper), and $Re_{dc} = 210 \pm 40$ in the sparse patch ($\phi = 0.02$). *Chen et al.* [2012] provided deposition data for a sparse (Case 16) and dense (Case 17) circular patch of the same ϕ, so we assume the same Re_{dc} ($= 132 \pm 12$ dense patch and $= 210 \pm 40$ sparse patch). For these studies deposition within the patch was compared to deposition observed in the bare channel upstream of the patch, and $u_* = \sqrt{c_f} U_0$. Categories of net deposition were plotted in the parameter space of normalized stem Reynolds number, $Re_{d(local)}/Re_{dc}$, and normalized channel shear velocity, u_*/u_{*c} (Figure 7). The threshold $Re_{d(local)}/Re_{dc} = 1$ is marked by a vertical grey box which spans the uncertainty transferred from the uncertainty in Re_{dc}. The threshold $u_*/u_{*c} = 1$ is marked by a horizontal dashed line. The region $Re_{d(local)}/Re_{dc} < 1$ and $u_*/u_{*c} > 1$ satisfies both criteria for enhanced deposition within a patch: the absence of stem turbulence ($Re_{d(local)}/Re_{dc} < 1$) and the presence of resuspension (sediment supply) in the open channel ($u_*/u_{*c} > 1$). 83% of the red points, which indicated net deposition greater than the open channel control, fell in this parameter space, consistent with the stated criteria. Some red points fell a bit above $Re_{d(local)}/Re_{dc} = 1$, which may be attributed to the imprecision in defining Re_{dc}. Blue points indicated deposition less than the open channel control, and 93% of blue points fell in the region $Re_{d(local)}/Re_{dc} \geq 1$ regardless of u_*/u_{*c}. This indicated that the presence of stem turbulence ($Re_{d(local)}/Re_{dc} \geq 1$) diminished net deposition within the patch.

4. Discussion

Previous studies provide additional examples consistent with the classification given in Figure 7. First, *Sand-Jensen* [1998] reported enhanced net deposition within finite patches of natural vegetation. Sufficient data for *Elodea Canadensis* was available to add those measurements to Figure 7 (shown as stars). The diameter (d) of *Elodea canadensis* stems was given as ≤ 7 mm, and the velocity measured at three positions in the patch was 0.9, 0.7, 0.6 cm s^{-1} [*Sand-Jensen*, 1998, Table 1], so that $Re_d = 40$ to 60. Assuming $Re_{dc} = 120$, $Re_{d(local)}/Re_{dc} < 1$ within the *Elodea*, such that stem-turbulence should not be present in the patch. The channel velocity was $U_0 = 20$ to 60 cm s^{-1}, the water depth was $H = 0.4$ to 0.8 m, and the grain size in the open channel (1 m upstream of patch) was $d_{50} = 0.3$ mm. The grain size can be used to estimate the bed friction coefficient [*Julien*, 1995, equation (6.14) and Table 6.1], yielding $u_* = 1.3$ to 3.2 cm s^{-1}. The grain size within the patch was $d_{50} = 0.2$ mm (Figure 4) [*Sand-Jensen*, 1998]. Since we are interested in the deposition of this grain size into the patch, we find the critical shear velocity for this grain size following *Julien* [1995, equation (7.4)], $u_{*c} = 0.9$ cm s^{-1}, such that $u_*/u_{*c} = 1.4$ to 3.6 (mean value = 2.5). The *Sand-Jensen* measurements fall in the quadrant of $Re_{d(local)}/Re_{dc} < 1$ and $u_*/u_{*c} > 1$ in Figure 7 (stars), and consistent with this net deposition within the patch was enhanced, relative to the adjacent bare bed.

Second, *Follett and Nepf* [2012] considered a circular patch of emergent vegetation in a sand bed. For all flow conditions erosion was observed within the patch, relative to the surrounding bare bed [*Follett and Nepf*, 2012, Figure 8], and this was attributed to stem-generated turbulence. Specifically, the magnitude of net erosion within the patch was positively correlated with estimates of stem-generated *TKE*. *Kim et al*. [2015] also considered a finite region of model vegetation in a sand bed. They compared flow conditions for which $u_*/u_{*c} > 1$ and $u_*/u_{*c} < 1$. When $u_*/u_{*c} < 1$ erosion was observed within the leading edge of the patch [*Kim et al*., 2015, Figure 9]. This could be attributed to the presence of stem-scale turbulence ($Re_{d(local)} > Re_{dc}$) and the lack of sediment supply from the channel ($u_*/u_{*c} < 1$). In contrast, when $u_*/u_{*c} > 1$ providing a sediment supply to the patch, both erosion and deposition, relative to the bare channel, was observed within the patch [*Kim et al*., 2015, Figure 12]. Erosion was observed near the leading edge, where higher velocity promoted stem-generated turbulence, and deposition was observed farther from the leading edge, where reduced velocity precluded stem-generated turbulence.

Balke et al. [2012] described the variation in the morphology of salt marsh tussocks (circular regions of pioneer vegetation) as a function of the depositional environment, i.e., whether the surrounding region was accreting or eroding, and sediment type (sandy versus silty), which they associated with high (sandy) and low (silty) hydrodynamic energy (waves and currents). For accreting conditions, the tussocks were depressed relative to the surrounding bed in high energy (sandy) regions, but elevated in a dome relative to the surrounding bed in low energy (silty) regions. *Balke et al*. [2012] attributed the difference in morphology (depression versus dome) to the level of stem-generated turbulence within the tussock, which was more likely to be present in high energy environments for which current within the tussock would also be higher. The two limits of behavior (depression versus dome) are consistent with the classification given in Figure 7. Specifically, for accreting regions sediment supply to the patch is not limited, which is analogous to $u_*/u_{*c} > 1$ in Figure 7, denoting that a suspended sediment supply was available for the patch. Enhanced deposition within the patch (dome morphology) occurred in low energy environments, for which $Re_{d(local)}/Re_{dc} < 1$ was likely, and reduced deposition within the patch (depression morphology) occurred in high energy environments, for which $Re_{d(local)}/Re_{dc} > 1$ was likely. Both of these are consistent with Figure 7. For eroding environments, the tussock was also raised, relative to the surrounding bed, but the difference in elevation was not attributed to enhanced deposition within the tussock, but instead to enhanced erosion at the edge, which was associated with the flow diversion around the tussock and the sediment binding achieved by the roots. These processes are not captured by the classification in Figure 7. We note this to emphasize that a variety of biotic and abiotic processes contribute to morphologic evolution (as discussed in *Balke et al*. [2012]), and that Figure 7 only captures the abiotic processes of flow modification and sediment transport.

The classification shown in Figure 7 can be used to evaluate the potential for in-patch particle deposition in the field. For a given channel velocity, patch width, and stem density, equations (4–6) can be used to estimate the velocity within a patch, and specifically the length-scale (L_t) for which $Re_d < Re_{dc}$. Patches of length $L > L_t$ produce conditions favorable for in-patch deposition, i.e., absence of stem-generated turbulence. The channel velocity and grain size would be used to evaluate the potential for sediment supply to the patch ($u_*/u_{*c} >$ or < 1). The same method could be applied in tidal systems, if the time-scale for tidal variation is long compare to the flow development time-scale over the patch (L/u), which generally would be true. In this case, the system could be evaluated as a sequence of quasi-steady flow conditions. For submerged patches, the height of the patch (h) introduces another length-scale that influences the velocity adjustment (X_D). For high-flow blockage, channel-spanning, submerged patches, *Chen et al*. [2013] observed $X_D \approx 7h$. For submerged patches of finite width, the smaller dimension (D versus h) should control the flow adjustment. Specifically, for high-flow blockage (C_Dah and $C_DaD > 4$), equations (4–6) would apply, with $X_D = \min(3.5D, 7h)$. For low-flow blockage patches, turbulent stress penetration into the patch must also be considered in the estimation of in-patch velocity (see discussion in *Rominger and Nepf* [2011]).

5. Conclusions

Laboratory experiments identified the threshold for stem-generated turbulence within emergent vegetation and explored how channel velocity influenced the pattern of net deposition around and within the patch. The presence of resuspension within the channel ($u_* > u_{*c}$) was a necessary condition to produce spatial

variation in the net deposition around the patch. For $u_* > u_{*c}$ resuspension adjacent to the patch both reduced net deposition adjacent to the patch and enhanced net deposition within the wake behind the patch, because particles put back into suspension from the adjacent region became available to deposit in the wake. Two criteria were necessary for enhanced net deposition inside the patch, relative to the bare-channel: resuspension in the channel ($u_* > u_{*c}$), and the absence of stem-scale turbulence ($Re_{d(local)} < Re_{dc}$) within the patch. Previous laboratory and field studies observed patterns of net deposition and erosion within patches that were consistent with these criteria. However, we caution that the physical mechanisms of flow modification and sediment transport captured by the parameterization of u_* and Re_d may not represent all relevant processes that determine the morphology in vegetated landscapes.

Acknowledgments
This material is based upon work supported by NSF grant EAR-1414499. Any opinions, findings, and conclusions in this paper are those of author(s) and do not necessarily reflect the views of the National Science Foundation. We thank Jiarui Lei for his help in imaging the tracer experiments. Chao Liu was supported by the China Scholarship Council and the National Natural Science Foundation of China (51479128). Data presented in this paper are available upon request from the authors.

References

Asaeda, T., P. I. A. Gomes, K. Sakamoto, and M. H. Rashid (2011), Tree colonization trends on a sediment bar after a major flood, *River Res. Appl.*, *27*(8), 976–984.
Balke, T., P. C. Klaassen, A. Garbutt, D. van der Wal, P. M. J. Herman, and T. J. Bouma (2012), Conditional outcome of ecosystem engineering: A case study on tussocks of the salt marsh pioneer Spartina anglica, *Geomorphology*, *153*, 232–238.
Bennett, S., T. Pirim, and B. Barkdoll (2002), Using simulated emergent vegetation to alter stream flow direction within a straight experimental channel, *Geomorphology*, *44*, 115–126.
Bouma, T. J., L. A. Van Duren, S. Temmerman, T. Claverie, A. Blanco-Garcia, T. Ysebaert, and P. M. J. Herman (2007), Spatial flow and sedimentation patterns within patches of epibenthic structures: Combining field, flume and modelling experiments, *Cont. Shelf Res.*, *27*(8), 1020–1045.
Chambers, P. A., E. E. Prepas, M. L. Bothwell, and H. R. Hamilton (1989), Roots versus shoots in nutrient uptake by aquatic macrophytes in flowing waters, *Can. J. Fish. Aquat. Sci.*, *46*, 435–439.
Chen, Z., A. Ortiz, L. Zong, and H. Nepf (2012), The wake structure behind a porous obstruction and its implications for deposition near a finite patch of emergent vegetation, *Water Resour. Res.*, *48*, W09517, doi:10.1029/2012WR012224.
Chen, Z., C. Jiang, and H. Nepf (2013), Flow adjustment at the leading edge of a submerged aquatic canopy, *Water Resour. Res*, *49*, 5537–5551, doi:10.1002/wrcr.20403.
Cheng, N. S. (1997), Simplified settling velocity formula for sediment particle, *J. Hydraul. Eng.*, *123*(2), 149–152.
Clarke, S. (2002), Vegetation growth in rivers: influences upon sediment and nutrient dynamics, *Prog. Phys. Geogr.*, *26*(2), 159–172.
Cotton, J. A., G. Wharton, J. A. B. Bass, C. M. Heppell, and R. S. Wotton (2006), The effects of seasonal changes to in-stream vegetation cover on patterns of flow and accumulation of sediment, *Geomorphology*, *77*(3-4), 320–334.
Follett, E. M., and H. M. Nepf (2012), Sediment patterns near a model patch of reedy emergent vegetation, *Geomorphology*, *179*, 141–151.
Goring, D. G., and V. I. Nikora (2002), Despiking acoustic Doppler velocimeter data, *J. Hydraul. Eng.*, *128*(1), 117–126.
Gurnell, A. (2014), Plants as river system engineers, *Earth Surf. Processes Landforms*, *39*(1), 4–25.
Gurnell, A. M., and G. E. Petts (2002), Island-dominated landscapes of large floodplain rivers, a European perspective, *Freshwater Biol.*, *47*(4), 581–600.
Gurnell, A. M., W. Bertoldi, and D. Corenblit (2012), Changing river channels: The roles of hydrological processes, plants and pioneer fluvial landforms in humid temperate, mixed load, gravel bed rivers, *Earth Sci. Rev.*, *111*(1-2), 129–141.
Heppell, C. M., G. Wharton, J. A. C. Cotton, J. A. B. Bass, and S. E. Roberts (2009), Sediment storage in the shallow hyporheic of lowland vegetated river reaches, *Hydrol. Processes*, *23*(15), 2239–2251.
Jones, J. I., A. L. Collins, P. S. Naden, and D. A. Sear (2012), The relationship between fine sediment and macrophytes in rivers, *River Res. Appl.*, *28*(7), 1006–1018, doi:10.1002/rra.1486.
Julien, P. Y. (1995), *Erosion and Sedimentation*, Cambridge Univ. Press, N. Y.
Kim, H. S., I. Kimura, and Y. Shimizu (2015), Bed morphological changes around a finite patch of vegetation, *Earth Surf. Processes Landforms*, *40*(3), 375–388, doi:10.1002/esp.3639.
Liu, D., P. Diplas, J. D. Fairbanks, and C. C. Hodges (2008), An experimental study of flow through rigid vegetation, *J. Geophys. Res.*, *113*, F04015, doi:10.1029/2008JF001042.
Meire, D. W. S. A., J. M. Kondziolka, and H. M. Nepf (2014), Interaction between neighboring vegetation patches: Impact on flow and deposition, *Water Res. Res.*, *50*, 3809–3825, doi:10.1002/2013WR015070.
Naden, P., P. Rameshwaran, O. Mountford, and C. Robertson (2006), The influence of macrophyte growth, typical of eutrophic conditions, on river flow velocities and turbulence production, *Hydrol. Processes*, *20*(18), 3915–3938.
Naiman, R. J., H. Decamps, and M. Pollock (1993), The role of riparian corridors in maintaining regional biodiversity, *Ecol. Appl.*, *3*(2), 209–212.
Nepf, H. M. (1999), Drag, turbulence, and diffusion in flow through emergent vegetation, *Water Resour. Res*, *35*(2), 479–489.
Norberg, C. (1994), An experimental investigation of the flow around a circular cylinder: influence of aspect ratio, *J. Fluid Mech.*, *258*, 287–316.
Ortiz, A. C., A. Ashton, and H. Nepf (2013), Mean and turbulent velocity fields near rigid and flexible plants and the implications for deposition, *J. Geophys. Res. Earth Surf.*, *118*, 2585–2599, doi:10.1002/2013JF002858.
Ricardo, A. M., K. Koll, M. J. Franca, A. J. Schleiss, and R. M. L. Ferreira (2014), The terms of turbulent kinetic energy budget within random arrays of emergent cylinders, *Water Resour. Res.*, 4131–4148, doi:10.1002/2013WR014596.
Rominger, J. T., and H. M. Nepf (2011), Flow adjustment and interior flow associated with a rectangular porous obstruction, *J. Fluid Mech.*, *680*, 636–659.
Sand-Jensen, K. (1998), Influence of submerged macrophytes on sediment composition and near-bed flow in lowland streams, *Freshwater Biol.*, *39* (4), 663–679.
Sukhodolov, A. N., and T. A. Sukhodolova (2009), Case study: Effect of submerged aquatic plants on turbulence structure in a lowland river, *J. Hydraul. Eng.*, *136*(7), 434–446.
Takemura, T., and N. Tanaka (2007), Flow structures and drag characteristics of a colony-type emergent roughness model mounted on a flat plate in uniform flow, *Fluid Dyn. Res.*, *39*(9-10), 694–710.
Tanino, Y., and H. M. Nepf (2008a), Lateral dispersion in random cylinder arrays at high Reynolds number, *J. Fluid Mech.*, *600*, 339–371.

Tanino, Y., and H. M. Nepf (2008b), Laboratory investigation of mean drag in a random array of rigid, emergent cylinders, *J. Hydraul. Eng.*, *134*(1), 34–41.
Vandenbruwaene, W., et al. (2011), Flow interaction with dynamic vegetation patches: Implications for biogeomorphic evolution of a tidal landscape, *J. Geophys. Res.*, *116*, F01008, doi:10.1029/2010JF001788.
van Wesenbeeck, B. K., J. Van De Koppel, P. Mj Herman, and T. J Bouma (2008), Does scale-dependent feedback explain spatial complexity in salt-marsh ecosystems?, *Oikos*, *117*(1), 152–159.
White, B. L., and H. M. Nepf (2007), Shear instability and coherent structures in shallow flow adjacent to a porous layer, *J. Fluid Mech.*, *593*, 1–32.
Wood, P. J., and P. D. Armitage (1997), Biological effects of fine sediment in the lotic environment, *Environ. Manage.*, *21*(2), 203–217.
Wu, W., F. D. Shields, S. J. Bennett, and S. S. Y. Wang (2005), A depth-averaged, two-dimensional model for flow, sediment transport, and bed topography in curved channels with riparian vegetation, *Water Resour. Res.*, *41*, W03015, doi:10.1029/2004WR003730.
Zong, L. J., and H. Nepf (2010), Flow and deposition in and around a finite patch of vegetation, *Geomorphology*, *116*(3-4), 363–372.
Zong, L. J., and H. Nepf (2012), Vortex development behind a finite porous obstruction in a channel, *J. Fluid Mech.*, *691*, 368–391.